Mechanism of stepwise electron transfer in six-transmembrane epithelial antigen of the prostate (STEAP) 1 and 2

Kehan Chen[1,*], Lie Wang[1,*], Jiemin Shen[1], Ah-lim Tsai[2], Ming Zhou[1,#], Gang Wu[2,#]

[1] Verna and Marrs McLean Department of Biochemistry and Molecular Biology, Baylor College of Medicine, Houston, Texas 77030, United States

[2] Division of Hematology-Oncology, Department of Internal Medicine, University of Texas-McGovern Medical School, Houston, Texas 77030, United States

* These authors contributed equally

[#] Corresponding authors: gang.wu@uth.tmc.edu and mzhou@bcm.edu

Running title: Electron transfer mechanism of STEAP

Abstract

Six transmembrane epithelial antigen of the prostate (STEAP) is a family of four members, and all have a transmembrane domain with a conserved heme binding site. STEAP2 – 4, but not STEAP1, have an intracellular domain that binds to NADPH and FAD. STEAP2 – 4 show metal ion reductase activities, which led to the notion that STEAPs mediate electron transfer starting from NADPH on the intracellular side, through FAD and heme, and finally to a metal ion substrate on the extracellular side. However, the electron transfer chain has not been reconstructed with purified proteins for rigorous investigation. It is also unclear whether STEAP1 has metal ion reductase activity and if so, how electrons are transferred. We expressed and purified mammalian STEAP1 and 2, re-constructed the electron transfer chain *in vitro* and examined individual electron transfer steps. We find that the heme in both STEAP1 and 2 can transfer electrons to a metal ion substrate and that STEAP1 reduces the metal ion significantly faster than STEAP2. We determined the structure of STEAP2 by cryo-electron microscopy and find that its substrate binding site is less well ordered compared to the structures of STEAP1 and 4, which may explain its lower reductase activity. We also demonstrate that the FAD on STEAP2 becomes diffusible after reduction by NADPH. We show that STEAP1 can form an electron transfer chain with cytochrome b_5 reductase. These results establish a solid foundation for understanding the functions of STEAP1 and 2 in cells.

Introduction

Six transmembrane epithelial antigen of the prostate (STEAP) is a family of four membrane-embedded hemeproteins, STEAP1 – 4. Functions of STEAP2 – 4 have been examined in cell-based assays that demonstrated their ability to reduce extracellular ferric and cupric ions,[1, 2] and implicated their involvement in the endosomal transferrin cycle, and trafficking and availability of iron and copper *in vivo*.[3, 4] STEAP2 – 4 are also found overexpressed in many types of cancer cells, suggesting their possible participation in cancer initiation, promotion, and progression.[5-7] However, cellular function of STEAP1, whose abnormally high level of expression in prostate and prostate cancer cells led to the discovery and namesake of the family, remains unresolved.

STEAP proteins belong to a large superfamily of membrane-embedded reductases which include mammalian NADPH oxidases (NOX) and dual oxidases (DUOX), and bacterial and yeast ferric reductases (FRE).[8] This superfamily of proteins all have a transmembrane domain (TMD) composed of six transmembrane helices (TM). The structures of NOX and DUOX show that their TMD binds two heme prosthetic groups, each ligated to a pair of conserved histidine residues from TMs 3 and 5; one heme is close to the intracellular side and the other close to the extracellular side of the membrane.[9-11] An intracellular redox domain (RED) in NOX or DUOX binds to both NADPH and FAD to fulfill the electron transfer function. Structures of STEAP1 and STEAP4 were reported previously.[12, 13] Interestingly, STEAPs have only a single pair of conserved histidine residues from TMs 3 and 5 that ligate to one heme near the extracellular side of the membrane. STEAP4 has a homotrimeric structure and the FAD binds in an extended conformation straddling the TMD and RED domains from different protomers.[13] The isoalloxazine ring of a FAD occupies a position equivalent to the heme on the intracellular side

of NOX and DUOX.[9, 10, 13] However, this conformation of FAD places its isoalloxazine ring ~19 Å from the closest NADP(H) in the RED, which raises the question of how NADPH transfers hydride to FAD. A "FAD-shuttling" mechanism was proposed in which the bound FAD switches between the extended conformation observed in the structure and a "folded" conformation with the isoalloxazine ring aligned in close proximity to the NADPH nicotinamide ring.[13] However, there has been no experimental evidence supporting the shuttling of FAD isoalloxazine moiety. In addition, STEAP1, which lacks a RED that mediates electron transfer between NADPH and FAD, remains enigmatic for its definitive redox function. We have shown previously that chemically reduced heme in STEAP1 can efficiently reduce ferric/cupric substrates, and that STEAP1 could form a heterotrimer with STEAP2,[14] but it is unclear whether STEAP1 can form a competent electron transfer chain from NADPH.

In this study, we established fully functional electron transfer chains in both STEAP1 and STEAP2 and determined the cryo-electron microscopy (cryo-EM) structure of STEAP2 that may explain its low activity towards metal ion substrates. We also found that the FAD on STEAP2 becomes diffusible, which supports the "FAD-shuttling" hypothesis proposed in STEAP4 by Oosterheert et al.[13]

Results

Spectroscopy of STEAP2. Purified STEAP2 elutes as a single peak from a size-exclusion chromatography column and the elution volume corresponds to a molecular weight between ~100 – 150 kD (Fig. S1A), suggesting that STEAP2 forms a homotrimer. A prominent heme absorption peak is present in the purified STEAP2, and the heme content typically ranges from 70 – 90 %. FAD is also detected in the purified STEAP2; however, its level varies and is less

than 20 % based on the fluorescence of FAD released from denatured STEAP2. No NADP(H) can be detected in the purified STEAP2, suggesting that its association with STEAP2 is more transient than either heme or FAD.

The ferric heme in STEAP2 shows a Soret band at 413 nm and broad unresolved α/β bands centered around 550 nm (Fig. S1B). Upon dithionite reduction, the Soret band shifts to 427 nm and the α and β bands are well resolved at 560 and 532 nm, respectively (Fig. S1B). These UV-Vis spectral features are consistent with a bis-imidazole ligated *b*-type cytochrome. We further characterized the heme using magnetic circular dichroism (MCD) spectroscopy. The MCD spectrum of ferric STEAP2 (STEAP2(Fe(III))) shows strong Soret signals between 404 nm to 419 nm and no high-spin charge-transfer signal at wavelength above 600 nm (Fig. S1C). On the other hand, the MCD spectrum of ferrous STEAP2 (STEAP2(Fe(II))) has a much weaker Soret band but a very strong α band from 554 nm to 562 nm (Fig. S1C), consistent with the intense A-term Faraday effect of a typical low-spin *b*-type heme. Combined, both UV-Vis and MCD data indicate that the heme is in the low-spin state in both STEAP2(Fe(III)) and STEAP2(Fe(II)). The rigid low-spin heme in STEAP2 is consistent with its role of mediating electron transfer.

Metal ion reduction by heme. A previous study shows that membrane fractions from cell expressing STEAP2 has metal ion reductase activity.[2] Here we measure the rate constant of electron transfer from STEAP2 heme to an iron substrate Fe^{3+}-NTA. We first prepared STEAP2(Fe(II)) by dithionite reduction. In the presence of 125 μM Fe^{3+}-NTA, STEAP2(Fe(II)) is oxidized in triphasic kinetics with rate constants, 2.4 s^{-1}, 6.3×10^{-2} s^{-1}, and 7.2×10^{-3} s^{-1}, respectively (Fig. 1A, the percentage of each phase is 35%, 22%, and 43%, respectively). The rate constants do not show dependence on [Fe^{3+}-NTA]. We also measured the rate constants of

STEAP1(Fe(II)) with Fe^{3+}-NTA. STEAP1(Fe(II)) is readily oxidized in biphasic kinetics (Fig. S2A) and the rate constants k_{obs} show linear dependence on [Fe^{3+}-NTA] (Fig. S2B). The rate of STEAP1(Fe(II)) oxidation by Fe^{3+}-NTA is similar to those by Fe^{3+}-EDTA or Fe^{3+}-citrate,[14] but the rates are significantly faster than STEAP2(Fe(II)) re-oxidation by Fe^{3+}-NTA (Fig. 1B).

Electron transfer chain in STEAP1 and STEAP2. We proceed to assemble the complete electron transfer chain in STEAP2 with NADPH and FAD. We first pre-incubated STEAP2 with stoichiometric amount of FAD and then reacted it anaerobically with NADPH (Fig. 2). The Soret peak of ferric heme (A_{413}) shifts to that of ferrous heme (A_{427}) while the α and β bands are well resolved at 560 nm and 532 nm, respectively, indicating reduction of the heme (Fig. 2). The spectra of the resolved spectral species correspond to those of STEAP2(Fe(III)) plus FAD and STEAP2(Fe(II)) with reduced FAD, respectively (Fig. 2, inset). The rate constant of the transition between the two resolved spectral species is 1.2 (± 0.2) × 10^{-3} s^{-1} (Fig. 2, inset). These results also suggest that the FAD reduction by NADPH and the heme reduction by reduced FAD are concomitant in STEAP2.

Since the residues interacting with the FAD isoalloxazine ring in STEAP2 (see below) and STEAP4 are largely conserved in STEAP1, we were curious whether the isoalloxazine ring of reduced FAD can bind STEAP1 TMD and reduce the heme. We prepared reduced FAD by titrating FAD with dithionite anaerobically. We found that the reduced FAD readily reduces STEAP1 (Fig. 3A) and the time courses show biphasic kinetics (Fig. 3B). The rate constants of both phases exhibit dependence on [FAD] and K_M is estimated to be 2.7 and 4.7 μM, respectively (Fig. 3B, inset). This result suggests that an electron transfer chain can be established in STEAP1 from reduced FAD to metal ion substrates.

STEAP1 reduction by b_5R. We proceed to examine whether STEAP1 can obtain electrons from

cytochrome b_5 reductase (b_5R), which utilizes NADH to reduce FAD and is known to partner with cytochrome b_5 to reduce many other hemeproteins and nonheme iron centers. We purified b_5R and prepared an anaerobic mixture STEAP1 and b_5R and then added NADH to initiate electron transfer. In the rapid-scan reaction of the STEAP1/b_5R mixture with NADH, the Soret absorbance of STEAP1(Fe(III)) (A_{413}) shifts to that of the ferrous heme (A_{427}) with well split α and β bands at 560 nm and 530 nm, respectively (Fig. 4A), demonstrating the reduction of the STEAP1 heme. Three spectral species, *A* – *C*, are resolved with the rate constants of 177.9 (± 35.3) s^{-1} (*A* to *B*) and 0.13 (± 0.006) s^{-1} (*B* to *C*), respectively. The spectral species *A* corresponds to STEAP1(Fe(III)) plus b_5R and species *C* is STEAP1(Fe(II)) with reduced b_5R, respectively (Fig. 4A, inset). On the other hand, the spectral intermediate *B* has decreased absorbance in 420 – 500 nm range compared to *A* but with little change in the Soret range (Fig. 4A, inset) indicating that *B* contains reduced FAD and ferric heme. The resolution of *B* is due to the fast b_5R reduction by NADH without significant electron transfer from the reduced FAD to STEAP1. The *B* to *C* conversion reflects the electron transfer from b_5R to STEAP1 (Fig. 4A). It is interesting to notice that b_5R reduces the heme in STEAP1 significantly faster than reduction of heme in STEAP2 by its own RED (Fig. 2).

We then measured the binding of b_5R to STEAP1 by biolayer interferometry assay (BLI). The BLI data shows that STEAP1 binds b_5R with a K_D of 5.9 μM (Fig. S3). While we do not have a structure of STEAP1 in complex with b_5R, we speculate that FAD on b_5R may partially dissociate to straddle between the two proteins (Scheme 1).

Cryo-EM structure of STEAP2. We determined the structure of STEAP2 using cryo-EM to an overall resolution of 3.2 Å. The quality of density map was sufficient to build all the major structural elements of STEAP2 *de novo* (Figs. S4&5). The N-terminal residues 1 – 27, C-

terminal residues 470 – 490, and residues 332 – 353 (loop between TM3 and 4) are not resolved in our EM map, likely due to high degree of flexibility (Fig. 5). Like STEAP4, STEAP2 has a domain-swapped homotrimer structure, where the RED of one protomer interacts with the TMD of a neighboring protomer (Fig. 5a & b). Similar to the structures of REDs in STEAP3 and STEAP4,[13, 15, 16] the RED in STEAP2 shows structural homology to archaeal $F_{420}H_2$:$NADP^+$ oxidoreductase (FNO). Overall, the structure of STEAP2 has a root mean squared deviation (RMSD) of 0.8 Å (Cα) to that of STEAP4.[13]

Heme, FAD, and $NADP^+$ are unambiguously resolved in the density map (Fig. 5c). The FAD molecule adopts an extended conformation (Fig. 6), as observed in STEAP4.[13] The FAD is ~10 Å away (edge-to-edge) from the heme and the side chain of Leu371 protrudes approximately midway in between (Fig. 6). The distance of the isoalloxazine ring of FAD to the nearest nicotinamide ring of $NADP^+$ is ~19 Å (Fig. 5e), which is too long for direct hydride transfer. We also found densities that likely correspond to a phospholipid and cholesterol. A POPC molecule was built between the TMDs of two neighboring protomers, and two cholesterol molecules were built on the periphery of each TMD (Fig. S4). These tightly bound lipid molecules may have relevant structural and functional roles in STEAP2.

STEAP1 reduction by STEAP2. To test whether the FAD in STEAP2 undergoes significant conformational change during the electron transfer (Scheme 1), we examined whether FAD from STEAP2 can be utilized by STEAP1. We prepared a mixture of STEAP2 (plus stoichiometric FAD) and STEAP1 and reacted the STEAP mixture with NADPH (Fig. 4B). In this reaction, the Soret absorbance shifts from 413 nm to 427 nm and finally a narrow peak is observed at 427 nm with no shoulder at 413 nm (Fig. 4B), indicating that heme in both STEAP2 and STEAP1 is fully reduced. In the same reaction mixture minus STEAP2, only minor auto-reduction of STEAP1 is

observed (Fig. S6), which is likely due to the slow reduction of FAD by NADPH. Only two spectral species are resolved from the reaction of STEAP1/STEAP2 mixture with NADPH, corresponding to STEAP(Fe(III)) plus FAD and STEAP(Fe(II)) plus reduced FAD, with a rate constant of 5.5×10^{-4} s^{-1} (Fig. 4B, inset). Our results indicate that STEAP2 can supply reduce FAD to initiate electron transfer in STEAP1.

The role of bulky Leu230 in electron transfer in STEAP1. The efficient electron transfer from b_5R to STEAP1 provided us a tool to test the hypothesis that the electron transfer in STEAPs is mediated by the bulky residue located halfway between the FAD and heme.[13] Such a bulky sidechain is relatively conserved in STEAPs, Leu230 in STEAP1, Leu371 in both STEAP2 (Fig. 6) and STEAP3, and Phe359 in STEAP4.[13] We mutated Leu230 in STEAP1 to glycine which does not have a sidechain and examined the electron transfer rate in L230G STEAP1 with b_5R. The L230G STEAP1 has identical UV-Vis spectra to these of the wild-type (WT), suggesting that the mutation does not perturb the heme binding (Fig. S7). L230G STEAP1 is reduced by b_5R with three spectral species, *A* – *C*, and the rate constants are 78.8 (± 22.6) s^{-1} (*A* to *B*) and 0.02 (± 0.01) s^{-1} (*B* to *C*) (Fig. 7, inset). Species *A* corresponds to L230G STEAP1(Fe(III)) and b_5R while species *C* represents L230G STEAP1(Fe(II)) and reduced b_5R (Fig. 7, inset). As in WT STEAP1, fast reduction of b_5R by NADH leads to the resolution of spectral intermediate *B*, which has decreased absorbance in 420 – 500 nm region but nearly unchanged Soret absorbance compared to *A*. On the other hand, the *B* to *C* conversion rate constant is much slower in L230G STEAP1 than in WT (Fig. 4A), indicating that the heme reduction by b_5R decreases significantly in L230G STEAP1. These results are consistent with Leu230 mediating electron transfer from FAD to heme in STEAP1.

Discussion

In this study, we constructed the electron transfer chains using purified STEAP1 and STEAP2 and determined the structure of STEAP2. Although STEAP isozymes are known to reduce metal ions in cell-based assays,[2] direct monitoring of the redox state changes in the cofactors or heme has not been reported and our study paves the way for rigorous interrogation of individual electron transfer steps for better understanding of both the mechanism and cellular functions of STEAPs.

We demonstrate that STEAP1 is capable of metal ion reduction and that STEAP1 can be reduced by an FAD-dependent reductase b_5R. These results define a potential cellular function of STEAP1 and raise an interesting perspective that other flavin-dependent reductases such as P450 reductase, methionine synthase reductase, and NADPH-dependent diflavin oxidoreductase 1 may also supply reduced FAD to STEAP1. These flavin-dependent reductases are ubiquitously expressed in cells and may be relevant to cancer progression and tumorigenicity; for example, high expression of b_5R isozyme 3 promotes colonization and metastasis in estrogen receptor-negative breast cancer.[17] Compared to STEAP2 – 4, the lack of a RED domain in STEAP1 may allow it to partner with a larger pool of flavin-dependent reductases. Alternatively, STEAP1 could assemble with STEAP2 to form a heterotrimer, as we have shown in a previous study,[14] to acquire FAD from the RED of a neighboring STEAP2 protomer.

The structure of STEAP2 suggests that its substrate binding site is less defined than other STEAP isozymes, indicated by the unresolved residues 332 – 353 between TM3 and 4. In the structures of STEAP1 and STEAP4, the corresponding residues form an extracellular loop by the substrate binding site,[12, 13] and presumably help substrate binding. The slow Fe^{3+}-NTA reduction by STEAP2 is likely due to poor substrate binding. These structural differences that lead to

substantially decreased reduction of metal ion substrates may imply the difference of native substrates between STEAP2 and other isozymes. The structure of STEAP2 shows that FAD assumes an extended conformation, like in STEAP4, that cannot receive hydride from NADPH, which is 19 Å away. The assembly of an intracellular RED with a membrane-embedded TMD observed in NOX, DUOX, and STEAPs naturally led to the notion that NADPH, FAD, and heme form an uninterrupted rigid electron-transfer chain that shuttles electron from the intracellular cellular NADPH to the extracellular substrates. While this may be true for NOX and DUOX, in which rapid supply of electrons to their extracellular substrates are essential to their biological functions, it may not apply similarly to STEAPs since it has only one heme in the TMD, and their electron transfer relies on shuttling of FAD. Our observations that FAD from STEAP2 can be utilized by STEAP1 is consistent with such relatively flexible structures.

Materials and Methods

Materials 4-(2-hydroxyethyl)-1-piperazineethanesulfonic acid (HEPES), 5-aminolevulinic acid (5-ALA), isopropyl β-D-1-thiogalactopyranoside (IPTG), phenylmethanesulfonyl fluoride (PMSF), $Fe(NO_3)_3$, hemin chloride, dithionite, 1-palmitroyl-2-oleoyl-glycero-3-phosphocholine (POPC), and nitrilotriacetic acid (NTA) were from Sigma-Aldrich (St. Louis, MO). Lauryl maltose neopentyl glycol (LMNG) and glyco-diosgenin (GDN) were from Anatrace (Maumee, OH).

Protein expression and purification. The human STEAP2 gene (NCBI accession number AAN04080.1) was codon optimized and cloned into a modified pFastBac Dual expression vector for production of baculovirus according to the Bac-to-Bac method (Thermo Fisher Scientific, Waltham, MA). P3 viruses were used to infect High Five (*Trichoplusia ni*) or Sf9 (*Spodoptera*

frugiperda) insect cells at a density of ~ 3 × 10^6 cells mL^{-1} in the media including 0.5 mM 5-aminolevulinic acid, 10 µM $FeCl_3$, and 5 µM hemin chloride. Infected cells were grown at 27 ºC for 48 – 60 h before harvest. Cell membranes were prepared using a hypotonic/hypertonic wash protocol as previously described.[18] Purified cell membrane pellets were then flash-frozen in liquid nitrogen for further use.

Purified membranes were thawed and homogenized in 20 mM HEPES, pH 7.5 buffer containing 150 mM NaCl, and then solubilized with 1.5% (w/v) LMNG at 4 ºC for 2 h. After solubilization, cell debris was removed by ultracentrifugation (55,000 × g for 45 min at 4 ºC), and hSTEAP2 was purified from the supernatant using cobalt-based Talon affinity resin (Clontech, Mountain View, CA). The C-terminal His_6-tag was cleaved with tobacco etch virus (TEV) protease at room temperature for 30 min. The protein was concentrated to around 5 mg mL^{-1} using an Amicon spin concentrator with a 100 kDa cut-off (Millipore, Burlington, MA), and then loaded onto a SRT-3C SEC-300 size-exclusion column (Sepax Technologies, Newark, DE) equilibrated with 20 mM HEPES buffer containing 150 mM NaCl and 0.01% (w/v) LMNG. For the sample used in the cryo-EM structural studies, the size-exclusion column was equilibrated with 20 mM HEPES buffer containing 150 mM NaCl and 0.02% GDN.

Rabbit STEAP1 (NCBI accession number NP_001164745.1) was expressed and purified following the method published previously.[14] The L230G STEAP1 mutation was introduced by the QuikChange method (Stratagene, CA) using the primers:

forward, 5’- CGTGGGACTGGCTATCGGCGCTTTGCTGGCTGTGAC-3’;

reverse, 5’- GTCACAGCCAGCAAAGCGCCGATAGCCAGTCCCACG-3’.

The cDNA of mouse cytochrome b_5 reductase (b_5R, UniProt Q3TDX8, soluble form, residues 24 – 301) was subcloned into a pET vector which appends a polyhistidine tag and a

tobacco etch virus (TEV) protease site to the N-terminus of the overexpressed protein. The expression of b_5R followed the previous protocol[19] and the cell media was supplemented with 100 μM FAD.

Electronic absorption and magnetic circular dichroism (MCD) spectroscopy. UV-Vis spectra of STEAP2 were recorded using a HP8453 diode-array spectrophotometer (Hewlett-Packard, Palo Alto, CA). The extinction coefficient of the heme was determined by pyridine hemochrome assay as published previously.[14] MCD spectra of STEAP2 were recorded with a Jasco J-815 CD spectropolarimeter (Tokyo, Japan) equipped with an Olis permanent magnet (Bogart, GA). The parameters for MCD measurements are spectral bandwidth, 5 nm; time constant, 0.5 s; scan speed, 200 nm/min. Each MCD spectrum was an average of 12 repetitive scans and the signal intensity is expressed in units of $M^{-1}cm^{-1}$ $tesla^{-1}$.

Cryo-EM structure determination of STEAP2. Quantifoil R1.2/1.3 Cu grids were glow-discharged in air for 15 s at 10 mA in a plasma cleaner (PELCO EasiGlow, Ted Pella, Inc., Redding, CA). Glow-discharged grids were prepared using Thermo Fisher Vitrobot Mark IV. Concentrated hSTEAP2 in the presence of FAD and $NADP^+$ (3.5 μl) was applied to each glow-discharged grid. After blotted with filter paper (Ted Pella, Inc.) for 4.0 s, the grids were plunged into liquid ethane cooled with liquid nitrogen. A total of 7509 micrograph stacks were collected using SerialEM[20] on a Titan Krios electron microscope (Thermo Fisher) at 300 kV with a Quantum energy filter (Gatan, Pleasanton, CA), at a nominal magnification of 105,000× and with defocus values of −2.5 μm to −0.8 μm. A K3 Summit direct electron detector (Gatan) was paired with the microscope. Each stack was collected in the super-resolution mode with an exposing time of 0.175 s per frame for a total of 50 frames. The dose was about 50 e^- per $Å^2$ for each stack. The stacks were motion-corrected with MotionCor2[21] and binned (2 × 2) so that the

pixel size was 1.08 Å. Dose weighting[22] was performed during motion correction, and the defocus values were estimated with Gctf.[23]

A total of 4,210,570 particles were automatically picked (RELION 3.1)[24-26] from the motion-corrected images and imported into cryoSPARC[27]. After 2 rounds of two-dimensional (2D) classification, a total of 91 classes containing 1,031,895 particles were selected. A subset of 12 classes containing 117,053 particles were selected for *ab initio* three-dimensional (3D) reconstruction, producing one good class with recognizable structural features and three bad classes with no distinct structural features. Both the good and bad classes were used as references in the heterogeneous refinement (cryoSPARC) and yielded a good class at 4.10 Å from 305,849 particles. Non-uniform refinement (cryoSPARC) was then performed with C3 symmetry and an adaptive solvent mask, producing a map with an overall resolution of 3.16 Å. Resolutions were estimated using the gold-standard Fourier shell correlation with a 0.143 cut-off[28] and high-resolution noise substitution.[29] Local resolution was estimated using ResMap.[30]

The structural model of STEAP2 was built based on the cryo-EM structure of STEAP4 (PDB ID: 6HCY),[13] and the side chains were adjusted based on the density map. Model building was conducted in Coot[31]. Structural refinements were carried out in PHENIX in real space with secondary structure and geometry restraints.[32] The EMRinger Score was calculated as described previously.[33]

STEAP reduction by NADPH. STEAP2, 2.3 μM, or a mixture of 1.1 μM STEAP2 and 0.9 μM STEAP1 was pre-incubated with 2.5 and 2.2 μM FAD in a tonometer, respectively. The solutions were made anaerobic by 5 anaerobic cycles, each with 30 s vacuum followed by argon sparging for 4.5 min. The stock solution of NADPH was made anaerobic by N_2 sparging. Anaerobic NADPH solution was injected into the anaerobic STEAP solution using an airtight

syringe and the spectral changes were monitored at room temperature using the HP 8453 spectrophotometer. The spectral changes were deconvoluted using the Pro-Kineticist program coming with the stopped-flow machine (see below).

Stopped-flow experiments. To measure the electron transfer rate from ferrous STEAP to ferric nitrilotriacetic acid (Fe^{3+}.NTA) substrate, anaerobic STEAP was first titrated to the ferrous state using dithionite and then reacted with Fe^{3+}.NTA on an Applied Photophysics model SX-18MV stopped-flow machine (Leatherhead, UK), which was placed in a COY anaerobic chamber (Grass Lake, MI). The time course of A_{427}, which reflects the oxidation of ferrous STEAP, was followed. Fe^{3+}-NTA was prepared with ferric nitrate and NTA based on a ratio of [Fe^{3+}]:[NTA] = 1:4. The rate constants of the redox reactions were obtained by fitting the time courses using a monophasic or a multiphasic exponential function.

The anaerobic protein mixture of STEAP1 and b_5R was reacted with NADH and the spectral changes were monitored using a rapid-scan diode-array accessory with the stopped-flow machine. In the reaction of STEAP1 with pre-reduced FAD, anaerobic FAD was titrated with dithionite to produce reduced FAD (likely in ionized form $FADH^-$ due to pKa = 6.7 of $FADH_2$). Part of the reduced FAD was re-oxidized due to the very negative redox potential of FAD, and the absorbance of re-oxidized FAD was subtracted as the background. The spectral changes were deconvoluted using the Pro-Kineticist program coming with the stopped-flow machine.

Octet Biolayer Interferometry. Biolayer Interferometry (BLI) assays were performed at 30 °C under constant shaking at 1000 rpm using an Octet system (FortéBio, Fremont, CA). STEAP1 was immobilized on amine reactive second-generation (AR2G) biosensors (Sartorius, Göttingen, Germany). The biosensor tips were activated for 5 min in 1-ethyl-3-[3-dimethylaminopropyl]carbodiimide hydrochloride (EDC) and 10 mM N-

hydroxysulfosuccinimide (Sulfo-NHS) before being loaded with STEAP1 at a concentration of 1 µg/mL for 10 min. The tips were then quenched in 1 M ethanolamine (pH 8.5) for 5 min and equilibrated in 20 mM HEPES, pH7.5 containing 150 mM NaCl, 0.1% LMNG, and 0.1% BSA to reduce non-specific binding. The tips were then transferred into wells containing various concentration of b_5R, 20, 10, 5, 2.5, 1.3, and 0.6 µM, for association and then back to the equilibration wells for dissociation. The binding curves were aligned and corrected with the channel with no analyst protein. The association and dissociation phases were fitted with a monophasic exponential function. The equilibrium responses (Req) in the association incubation were plotted against [b_5R] and fitted with a dose-response function to calculate the dissociation constant K_D of STEAP/b_5R complex.

Data and Materials Availability

The EM data and fitted model of human STEAP2 are deposited in the Electron Microscopy Data Bank (EMD-25775) and the RCSB Protein Data Bank (7TAI). Original data is available upon request, please contact gang.wu@uth.tmc.edu.

Author Contribution Statement

GW and MZ initiated and designed the project. KC and LW led the effort of protein production and structure determination and with help from JS and GW. JS prepared protein mutant and measured protein-protein binding affinity. GW designed and conducted spectroscopic measurements. All authors analyzed and interpreted the data. GW and MZ wrote the manuscript with inputs from all authors.

Competing Interests

The authors declare no competing interests.

Reference

[1] Grunewald, T. G., Bach, H., Cossarizza, A., and Matsumoto, I. (2012) The STEAP protein family: versatile oxidoreductases and targets for cancer immunotherapy with overlapping and distinct cellular functions, *Biol Cell 104*, 641-657.

[2] Ohgami, R. S., Campagna, D. R., McDonald, A., and Fleming, M. D. (2006) The Steap proteins are metalloreductases, *Blood 108*, 1388-1394.

[3] Knutson, M. D. (2007) Steap proteins: implications for iron and copper metabolism, *Nutr Rev 65*, 335-340.

[4] Ji, C., and Kosman, D. J. (2015) Molecular mechanisms of non-transferrin-bound and transferring-bound iron uptake in primary hippocampal neurons, *J Neurochem 133*, 668-683.

[5] Hubert, R. S., Vivanco, I., Chen, E., Rastegar, S., Leong, K., Mitchell, S. C., Madraswala, R., Zhou, Y., Kuo, J., Raitano, A. B., Jakobovits, A., Saffran, D. C., and Afar, D. E. (1999) STEAP: a prostate-specific cell-surface antigen highly expressed in human prostate tumors, *Proc Natl Acad Sci U S A 96*, 14523-14528.

[6] Gomes, I. M., Santos, C. R., Socorro, S., and Maia, C. J. (2013) Six transmembrane epithelial antigen of the prostate 1 is down-regulated by sex hormones in prostate cells, *Prostate 73*, 605-613.

[7] Rocha, S. M., Barroca-Ferreira, J., Passarinha, L. A., Socorro, S., and Maia, C. J. (2021) *The Usefulness of STEAP Proteins in Prostate Cancer Clinical Practice*, Exon Publications, Brisbane, Australia.

[8] Zhang, X., Krause, K. H., Xenarios, I., Soldati, T., and Boeckmann, B. (2013) Evolution of the ferric reductase domain (FRD) superfamily: modularity, functional diversification, and signature motifs, *PLoS One 8*, e58126.

[9] Wu, J. X., Liu, R., Song, K., and Chen, L. (2021) Structures of human dual oxidase 1 complex in low-calcium and high-calcium states, *Nat Commun 12*, 155.

[10] Sun, J. (2020) Structures of mouse DUOX1-DUOXA1 provide mechanistic insights into enzyme activation and regulation, *Nat Struct Mol Biol 27*, 1086-1093.

[11] Liu, R., Song, K., Wu, J. X., Geng, X. P., Zheng, L., Gao, X., Peng, H., and Chen, L. (2022) Structure of human phagocyte NADPH oxidase in the resting state, *Elife 11*.

[12] Oosterheert, W., and Gros, P. (2020) Cryo-electron microscopy structure and potential enzymatic function of human six-transmembrane epithelial antigen of the prostate 1 (STEAP1), *J Biol Chem 295*, 9502-9512.

[13] Oosterheert, W., van Bezouwen, L. S., Rodenburg, R. N. P., Granneman, J., Forster, F., Mattevi, A., and Gros, P. (2018) Cryo-EM structures of human STEAP4 reveal mechanism of iron(III) reduction, *Nat Commun 9*, 4337.

[14] Kim, K., Mitra, S., Wu, G., Berka, V., Song, J., Yu, Y., Poget, S., Wang, D. N., Tsai, A. L., and Zhou, M. (2016) Six-Transmembrane Epithelial Antigen of Prostate 1 (STEAP1) Has a Single b Heme and Is Capable of Reducing Metal Ion Complexes and Oxygen, *Biochemistry 55*, 6673-6684.

[15] Sendamarai, A. K., Ohgami, R. S., Fleming, M. D., and Lawrence, C. M. (2008) Structure of the membrane proximal oxidoreductase domain of human Steap3, the dominant ferrireductase of the erythroid transferrin cycle, *Proc Natl Acad Sci U S A 105*, 7410-7415.

[16] Gauss, G. H., Kleven, M. D., Sendamarai, A. K., Fleming, M. D., and Lawrence, C. M. (2013) The crystal structure of six-transmembrane epithelial antigen of the prostate 4 (Steap4), a ferri/cuprireductase, suggests a novel interdomain flavin-binding site, *J Biol Chem 288*, 20668-20682.

[17] Lund, R. R., Leth-Larsen, R., Caterino, T. D., Terp, M. G., Nissen, J., Laenkholm, A. V., Jensen, O. N., and Ditzel, H. J. (2015) NADH-Cytochrome b5 Reductase 3 Promotes Colonization and Metastasis Formation and Is a Prognostic Marker of Disease-Free and Overall Survival in Estrogen Receptor-Negative Breast Cancer, *Mol Cell Proteomics 14*, 2988-2999.

[18] Bai, Y., McCoy, J. G., Levin, E. J., Sobrado, P., Rajashankar, K. R., Fox, B. G., and Zhou, M. (2015) X-ray structure of a mammalian stearoyl-CoA desaturase, *Nature 524*, 252-256.

[19] Shen, J., Wu, G., Tsai, A. L., and Zhou, M. (2020) Structure and Mechanism of a Unique Diiron Center in Mammalian Stearoyl-CoA Desaturase, *J Mol Biol 432*, 5152-5161.

[20] Mastronarde, D. N. (2005) Automated electron microscope tomography using robust prediction of specimen movements, *J Struct Biol 152*, 36-51.

[21] Zheng, S. Q., Palovcak, E., Armache, J. P., Verba, K. A., Cheng, Y., and Agard, D. A. (2017) MotionCor2: anisotropic correction of beam-induced motion for improved cryo-electron microscopy, *Nat Methods 14*, 331-332.

[22] Grant, T., and Grigorieff, N. (2015) Measuring the optimal exposure for single particle cryo-EM using a 2.6 A reconstruction of rotavirus VP6, *Elife 4*, e06980.

[23] Zhang, K. (2016) Gctf: Real-time CTF determination and correction, *J Struct Biol 193*, 1-12.

[24] Kimanius, D., Forsberg, B. O., Scheres, S. H., and Lindahl, E. (2016) Accelerated cryo-EM structure determination with parallelisation using GPUs in RELION-2, *Elife 5*.

[25] Scheres, S. H. (2012) RELION: implementation of a Bayesian approach to cryo-EM structure determination, *J Struct Biol 180*, 519-530.

[26] Scheres, S. H. (2015) Semi-automated selection of cryo-EM particles in RELION-1.3, *J Struct Biol 189*, 114-122.

[27] Punjani, A., Rubinstein, J. L., Fleet, D. J., and Brubaker, M. A. (2017) cryoSPARC: algorithms for rapid unsupervised cryo-EM structure determination, *Nat Methods 14*, 290-296.

[28] Rosenthal, P. B., and Henderson, R. (2003) Optimal determination of particle orientation, absolute hand, and contrast loss in single-particle electron cryomicroscopy, *J Mol Biol 333*, 721-745.

[29] Chen, S., McMullan, G., Faruqi, A. R., Murshudov, G. N., Short, J. M., Scheres, S. H., and Henderson, R. (2013) High-resolution noise substitution to measure overfitting and validate resolution in 3D structure determination by single particle electron cryomicroscopy, *Ultramicroscopy 135*, 24-35.

[30] Kucukelbir, A., Sigworth, F. J., and Tagare, H. D. (2014) Quantifying the local resolution of cryo-EM density maps, *Nat Methods 11*, 63-65.

[31] Emsley, P., Lohkamp, B., Scott, W. G., and Cowtan, K. (2010) Features and development of Coot, *Acta Crystallogr D Biol Crystallogr 66*, 486-501.

[32] Adams, P. D., Afonine, P. V., Bunkoczi, G., Chen, V. B., Davis, I. W., Echols, N., Headd, J. J., Hung, L. W., Kapral, G. J., Grosse-Kunstleve, R. W., McCoy, A. J., Moriarty, N. W., Oeffner, R., Read, R. J., Richardson, D. C., Richardson, J. S., Terwilliger, T. C., and

Zwart, P. H. (2010) PHENIX: a comprehensive Python-based system for macromolecular structure solution, *Acta Crystallogr D Biol Crystallogr 66*, 213-221.

[33] Barad, B. A., Echols, N., Wang, R. Y., Cheng, Y., DiMaio, F., Adams, P. D., and Fraser, J. S. (2015) EMRinger: side chain-directed model and map validation for 3D cryo-electron microscopy, *Nat Methods 12*, 943-946.

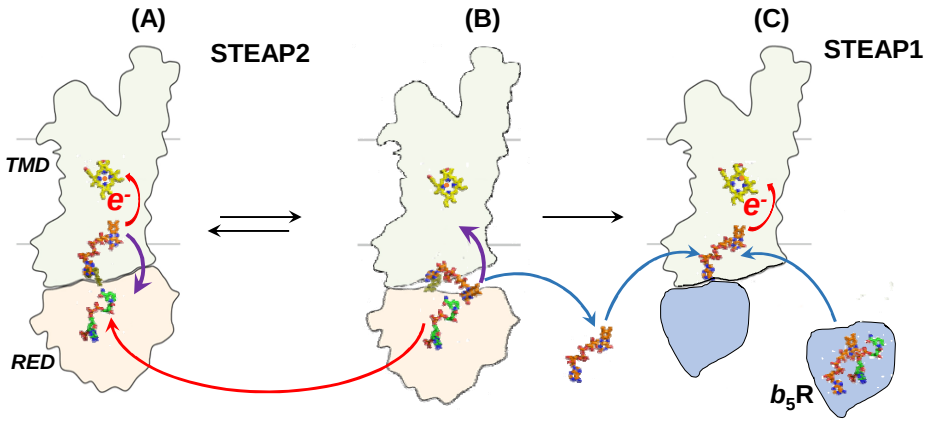

Scheme 1. Electron transfer pathways in STEAP1 and 2. (A) The FAD binds STEAP2 in an extended conformation straddling the TMD (grey) and RED (pink) domains of different protomers. The heme binds in the TMD and $NADP^+$ binds in the RED. (B) The hypothetic "folded" conformation of FAD stacks the isoalloxazine ring with the NADPH nicotinamide ring for hydride transfer. The switch between the two FAD conformations (purple arrow) is the "FAD-shuttling" mechanism (red arrow).[13] Significant structural changes may be required to accommodate the conformational switch of the FAD and such structural changes may allow the dissociation and rebinding of reduced FAD. (C) The reduced FAD generated in the REDs of STEAP2 or b_5R can reduce STEAP1 (blue arrow). Heme, yellow; FAD, orange; NAD(P)H, green.

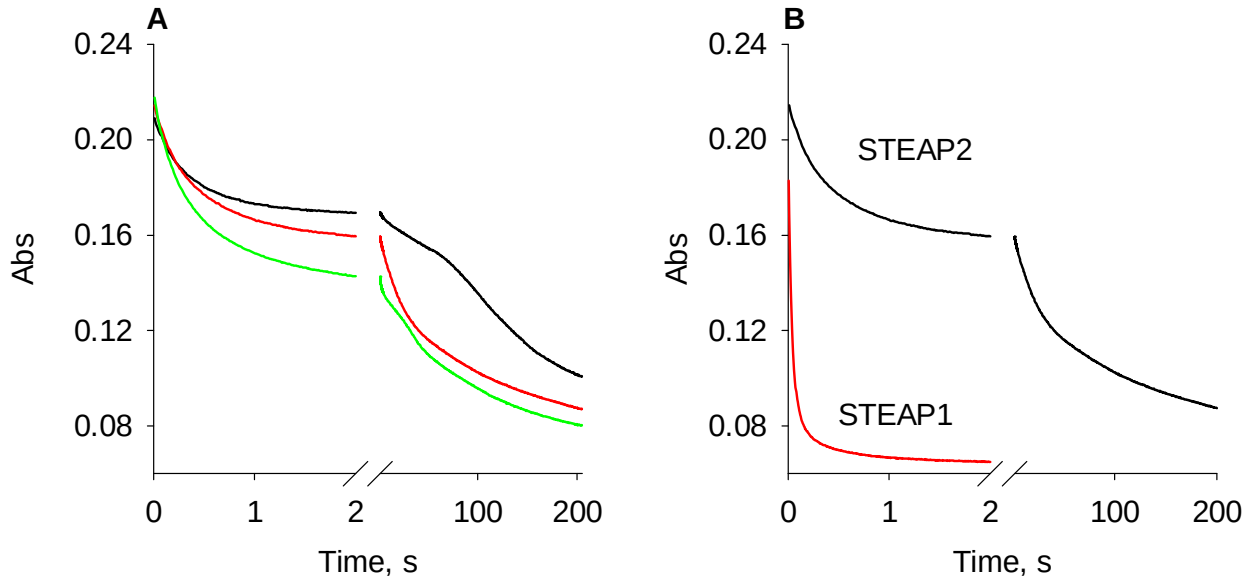

Figure 1. Re-oxidation of ferrous STEAP2 by Fe^{3+}-NTA. (A) The time courses of A_{427} in the reactions of 1.1 μM STEAP2(Fe(II)) with 75 (black), 125 (red), and 175 μM Fe^{3+}-NTA (green). (B) Comparison between the kinetics of STEAP2(Fe(II)) and STEAP1(Fe(II)) with 125 μM Fe^{3+}-NTA.

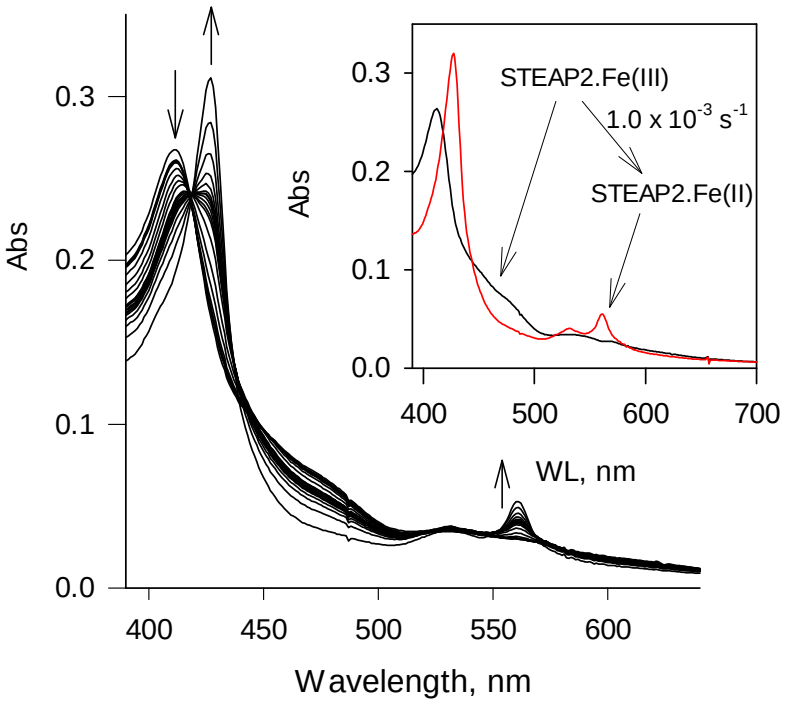

Figure 2. Heme reduction in STEAP2. (A) STEAP2, 2.3 μM, is pre-incubated with 2.5 μM FAD and reacted anaerobically with 45 μM NADPH. The direction of spectral change is indicated by the arrows. Inset, the resolved spectral species by deconvolution and the conversion rate constant. Black: STEAP2(Fe(III)) with FAD and red, STEAP2(Fe(II)) with reduced FAD.

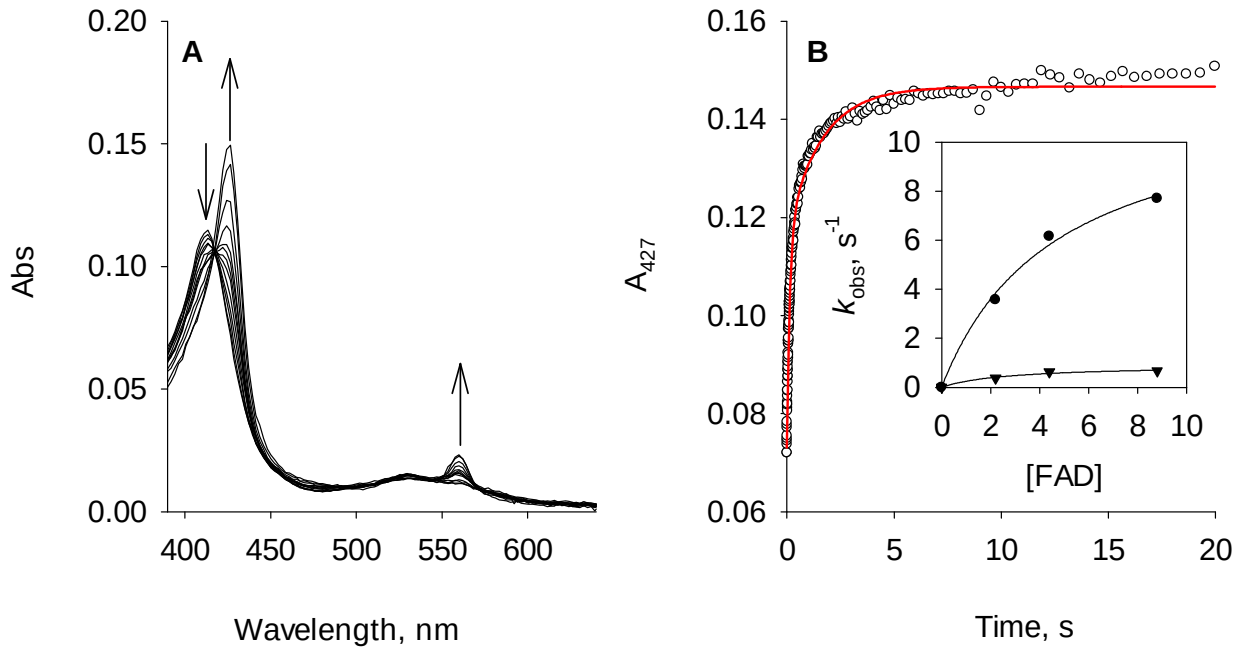

Figure 3. Anaerobic rapid-scan reaction of STEAP1 with reduced FAD. (A) Rapid-scan reaction of 1.1 μM STEAP1 with 4.5 μM pre-reduced FAD. (B) The time course of A_{427}, the Soret absorbance of ferrous heme, extracted from rapid-scan data. Red: biphasic exponential fit with rate constants of 7.7 (± 0.30) and 0.67 (± 3.4) × 10^{-2} s^{-1}, respectively (n = 3). Inset, the dependence of the fast phase (dot) and slow phase (triangle) rate constants on [FAD]. Lines, fit with equation $k = k_{max} * [FAD]/(K_M + [FAD])$.

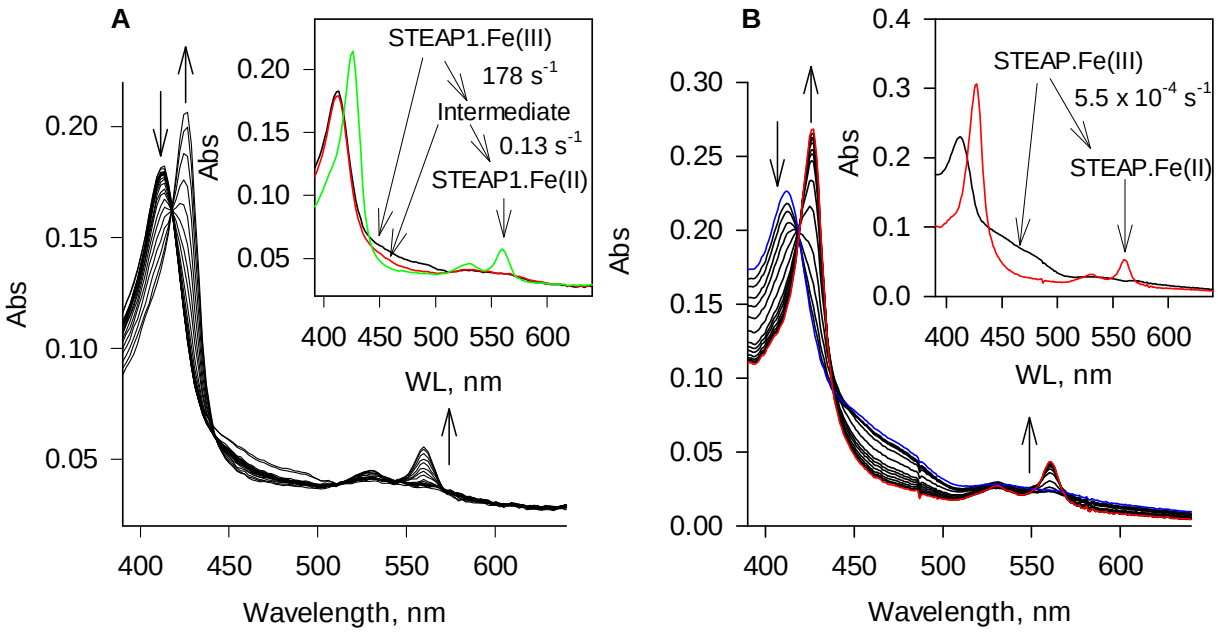

Figure 4. Reduction STEAP1 by FAD-dependent reductases. (A) The rapid-scan reaction of 1.5 μM STEAP1 and 1.5 μM b_5R with 10 μM NADH. The arrows indicate the direction of the spectral change. Inset: the resolved spectral species and the conversion rate constants. Black, STEAP1(Fe(III))/b_5R; red, a spectral intermediate, and green, STEAP1(Fe(II))/reduced b_5R. (B) The spectral changes in the reaction of a mixture of 1.1 μM STEAP2 and 0.9 μM STEAP1 (plus 2.2 μM FAD) with 60 μM NADPH. The direction of the spectral changes is indicated by the arrows. Blue, the spectrum captured at the start of the reaction; red, the spectrum after 1 hr reaction. Inset, the resolved spectral species by deconvolution and the conversion rate constant. Black, STEAP(Fe(III)) and red, STEAP(Fe(II)).

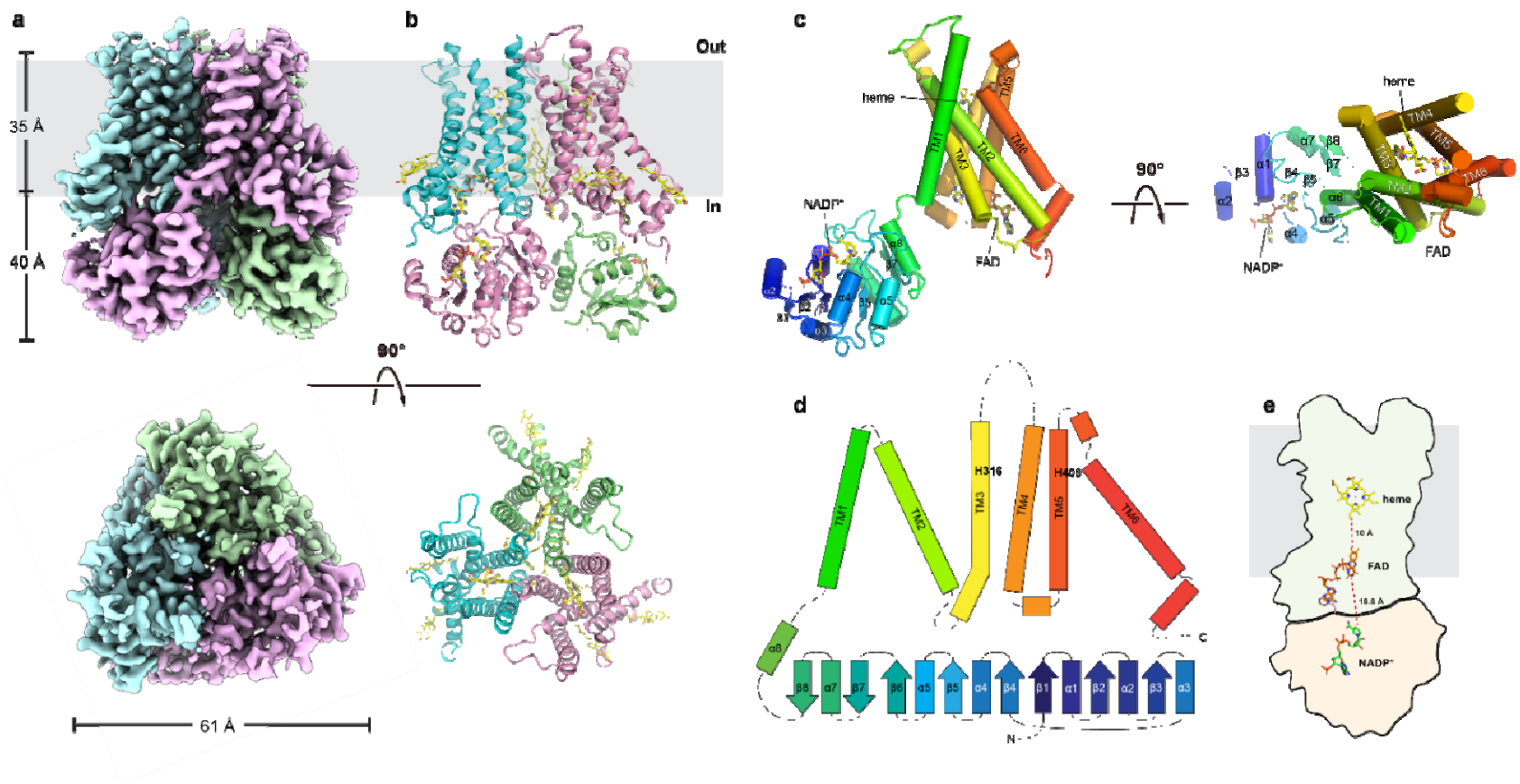

Figure 5. Cryo-EM structure of STEAP2. The sharpened density map (a) and cartoon presentation (b) for STEAP2 homotrimer. Top, the side view of STEAP2 homotrimer, and the grey bar represents the membrane; “in”, the intracellular side and “out’, the extracellular side. Bottom, the top view of STEAP2 homotrimer from the extracellular side. (c) The structure of one STEAP2 protomer. Left, side view and right, top view from the extracellular side. (d) The topographic representation of the secondary structural elements. The helices and β strands are represented by bars and arrows respectively. Dashed lines represent the unresolved

segments. (e) The schematic representation of the spatial relationship of $NADP^+$, FAD, and heme. TMD, grey shade and RED, pink shade.

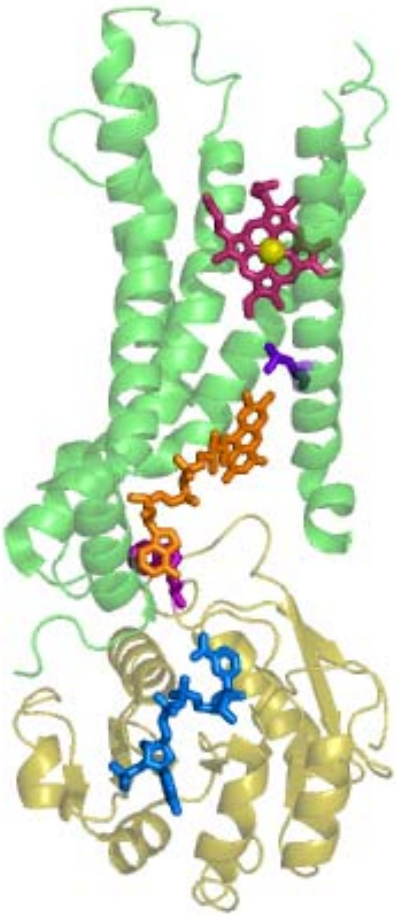

Figure 6. The FAD in STEAP2. The FAD (orange) binds STEAP2 in an extended conformation. Its isoalloxazine protrudes deep into the TMD domain (green) and the adenine ring stacks with Trp152 (pink) from the RED of a neighboring protomer (olive). Leu371 (purple) lies halfway between the isoalloxazine ring and heme (red, iron atom in yellow). $NADP^+$ in the RED is in blue.

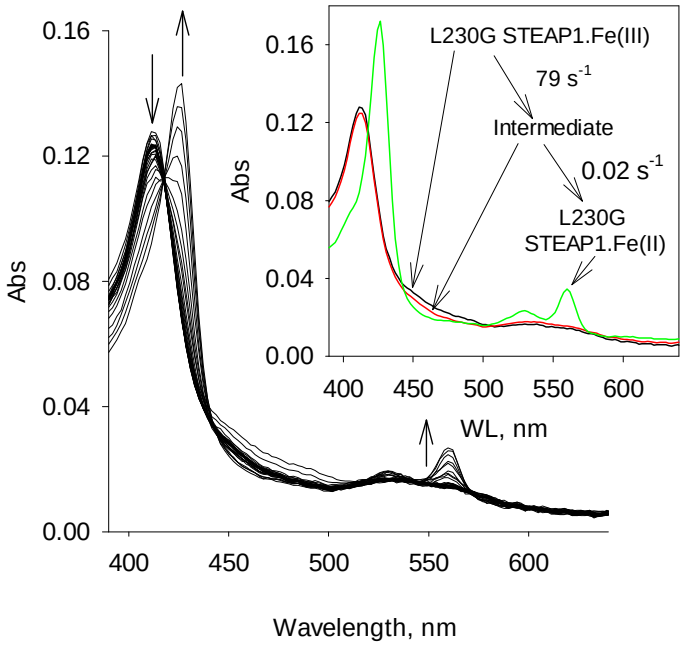

Figure 7. Reduction of L230G STEAP1 by *b*$_5$R. (A) L230G STEAP1 and *b*$_5$R were reacted with 10 μM NADH. The direction of spectral change is indicated by the arrows. Inset, the resolved spectral species by deconvolution and the rate constants. Inset: black, L230G STEAP1(Fe(III)/*b*$_5$R, red, a spectral intermediate, and L230G STEAP1(Fe(II))/reduced *b*$_5$R.